

Characterization of $(0.4)\text{Pb}_2(\text{In,Nb})\text{O}_6:(0.6)\text{Pb}(\text{Mg}_{1/3}\text{Nb}_{2/3})\text{O}_3$ relaxor ceramics

K.Z. Baba-kishi, C.W. Tai, J. Wang, C.L. Choy, and H.L.W. Chan
Department of Applied Physics and Materials Research Centre, The Hong Kong Polytechnic University, Hung Hom, Kowloon, Hong Kong

A.S. Bhalla
The Pennsylvania State University, Materials Research Laboratory, University Park, Pennsylvania 16802

(Received 21 June 2001; accepted 22 November 2001)

The results of the development and characterization of a new relaxor ceramic with nominal composition $(x)\text{Pb}_2(\text{In,Nb})\text{O}_6(1-x)\text{Pb}(\text{Mg}_{1/3}\text{Nb}_{2/3})\text{O}_3$ solid solution with $x = 0.4$ are reported. The structural characteristics, including the long-range and short-range order, forbidden reflections, and the existence of mixed ordering, were studied by transmission electron microscopy. The most prominent microstructural feature of this compound, which has composition variations in the micro- and nano-regions, was investigated. The presence of the pyrochlore phase and the complex arrangement of inclusions that originate from processing are illustrated. The electrical characteristics of the compound including pyroelectric, piezoelectric, electrostrictive and hysteresis properties are reported. Notable properties of the compound include a reduced hysteresis loop and nonlinear behavior at high field.

I. INTRODUCTION

The outstanding properties of piezoelectric crystals and ceramics can be related to the influence of morphotropic boundary phases and the development of domains. Morphotropic boundary phase is important in terms of composition, structure, and the division between at least two different crystal structures.¹ In $\text{Pb}(\text{Zr}_x\text{Ti}_{1-x})\text{O}_3$ (PZT), a morphotropic phase boundary separates the ferroelectric phase into two regions with distinct crystal structures: one is a tetragonal phase with Ti-rich composition, and the other is the rhombohedral phase with Zr-rich composition. In the region $\text{Zr}/\text{Ti} = 53/47$, the material has good piezoelectric properties, whereas in the solid solution regions 100/0 and 94/6, it is antiferroelectric with an orthorhombic structure, which lacks any piezoelectric property.² There is also an abrupt change of the lattice parameters close to the composition at the morphotropic phase boundary. Another material of significant complexity and importance is $(1-x)\text{Pb}(\text{Mg}_{1/3}\text{Nb}_{2/3})\text{O}_3:x\text{PbTiO}_3$, in which the morphotropic phase boundary is at $x = 0.35$. This material has an overall cubic symmetry according to x-ray and neutron diffraction studies but shows a complex domain configuration, which indicates the presence of a rhombohedral phase or an intermixing of both the tetragonal and rhombohedral phases.³⁻⁶

The crystallographic parameter often seen as a determining factor in the behavior of broad relaxation peak is structural ordering. A large number of Pb-based

ferroelectric compounds undergo some degree of structural ordering, which has been extensively studied.⁷⁻⁹ Some examples are $\text{Pb}_2(\text{Sc,Ta})\text{O}_6$, $\text{Pb}_2(\text{Mg,W})\text{O}_6$, and $\text{Pb}(\text{Mg}_{1/3}\text{Nb}_{2/3})\text{O}_3$, which possess complex crystal structures.

Studies on the fundamental crystal structures of the ferroelectric and pyroelectric $\text{Pb}_2\text{ScTaO}_6$ have been carried out.¹⁰⁻¹³ The structure of the relaxor $\text{Pb}_2\text{ScTaO}_6$ has been refined from high-resolution neutron time-of-flight powder diffraction data at both 400 and 4.2 K.¹¹ In $\text{Pb}_2\text{ScTaO}_6$ at 4.2 K, in the ferroelectric state, the structure is rhombohedral with a space group $R3$. According to the refinements, the structure of $\text{Pb}_2\text{ScTaO}_6$ in the ferroelectric state differs from the paraelectric state by cooperative ion shifts. The crystal structure of another ferroelectric oxide, $\text{Pb}_2\text{ScNbO}_6$, which is related to $\text{Pb}_2\text{ScTaO}_6$, has also been studied in a similar manner to that of $\text{Pb}_2\text{ScNbO}_6$.¹² The coordination polyhedra contain stereo-active lone electron pairs on Pb^{2+} . The Sc^{3+} and Ta^{5+} ions are shifted away from the centers of their respective octahedra towards the octahedral faces. These studies now enable a better understanding of the ways ferroelectric phase transition takes place in both $\text{Pb}_2\text{ScTaO}_6$ and $\text{Pb}_2\text{ScNbO}_6$.

By mixing $\text{Pb}_2(\text{In,Nb})\text{O}_6$ (PIN) with relaxor $\text{Pb}(\text{Mg}_{1/3}\text{Nb}_{2/3})\text{O}_3$ (PMN), we maintain the relaxor behavior across the phase diagram when the two materials are in the disordered states. The combination of PIN and PMN produces morphotropic boundary phases with

compositions $(x)\text{Pb}_2(\text{In,Nb})\text{O}_6:(1-x)\text{Pb}(\text{Mg}_{1/3}\text{Nb}_{2/3})\text{O}_3$, with $x = 0.10$ to 0.9 . These materials exhibit unusual structural and phase transition properties. PIN is antiferroelectric and is highly ordered at 120°C , whereas it is disordered at 90°C . The structural ordering and the consequent phase transition temperature are significantly altered with a decrease in PIN and a corresponding increase in the amount of PMN. The dielectric, electro-mechanical, structural, and phase transition properties of the morphotropic compositions that lie between PIN (100%) and PMN (100%) are unknown. The ceramics with composition PIN:PMN(40/60) are the subject of the present investigation because they show reduced hysteresis behavior. The compounds $(0.4)\text{PIN}:(0.6)\text{PMN}$ shall thereafter be referred to as PIM (40/60) for simplification.

II. EXPERIMENTAL

Stoichiometric powders were prepared by the Columbite method.¹⁴ The ceramics PIN and PMN were synthesized using the precursors In_2O_3 , Nb_2O_5 and MgCO_3 to form the required stoichiometric compounds.¹⁵ Calcination was performed and the resulting powders mixed and milled in acetone with ZrO_2 media. Eventually, pellets were pressed from the mixture, and the added binder removed. The pellets were then sintered at various temperatures. Specimens for transmission electron microscopy (TEM) were prepared by the conventional methods of lapping, grinding, and polishing, followed by Argon ion milling. A JEOL-2010 (Atom Tech. Ltd., UK) TEM operated at 200 kV was used in this study.

III. OBSERVATIONS

A. Characterization of the crystal structure and microstructure of PIM (40/60)

The ceramics of PIM (40/60) were characterized by TEM. The studies included the crystal structure, structural ordering, and intergranular inclusions. The TEM studies revealed the unique structural properties of PIM (40/60). Strong forbidden reflections often absent in Pb-based materials were observed, and the structural ordering associated with the development of a superstructure was ascertained.

The forbidden reflections $1/2\ 1/2\ 0$ and $1/2\ 0\ 0$ in many Pb-based ferroelectric ceramics are either completely absent or appear very weak. These reflections are generally illusive in that their presence is not predictable. To illustrate this, we use the case for $\text{Pb}_2\text{ScTaO}_6$. Figure 1(a) is an electron diffraction pattern recorded from a ceramic grain of $\text{Pb}_2\text{ScTaO}_6$ at room temperature. The pattern in Fig. 1(a) shows the reflections that can be indexed according to $Pm3m$ with lattice constant $0.407\ \text{nm}$.

However, the pattern also shows the forbidden reflections indexed as $1/2\ 1/2\ 0$. This reflection is often very difficult to record due its vanishing intensity. It is also often absent in x-ray and neutron diffraction patterns, though it has been seen in synchrotron x-ray patterns.¹⁰ Recent studies by neutron diffraction show that these reflections can be allowed if the structure is considered rhombohedral with space group $R3$, indicating that the crystals of $\text{Pb}_2\text{ScTaO}_6$ lack cubic symmetry in the paraelectric state.¹³ These reflections can also be permitted if there is mixed ordering of the B-sites cations. This is a very plausible and valid consideration since the possibility of 1:1 ordering is too ideal to exist in $\text{Pb}_2\text{ScTaO}_6$. One can easily consider the presence of Ta^{5+} or Sc^{3+} clusters in locally ordered configurations, allowing the weak and diffuse reflections to be created.

The electron diffraction pattern in Fig. 1(b) recorded from PIM(40/60) consistently showed the presence of a family of $1/2\ 1/2\ 0$ forbidden reflections, with exceptionally high intensities compared with those of $\text{Pb}_2\text{ScTaO}_6$. Upon heating to about 200°C and cooling to about -175°C of the PIM sample, no evidence of a change in the forbidden reflections was noted. In many Pb-based ferroelectric materials, new domain patterns appear on cooling to below the Curie temperature. In PIM, however, no domain patterns could be observed as the crystal was cooled or heated. The conclusion easily drawn from these patterns is that the structure is not a simple cubic structure with space group $Pm3m$. It appears that the possibility of mixed ordering the cations In, Nb, and Mg and the influence of Pb^{2+} displacements, especially at the presence of three elements In, Nb, and Mg, is significant. This is similar to the case of PIN.¹⁶ This then contributes to the fact that a rhombohedral phase with a possible $R3$ symmetry is operating the crystal structure.

Figure 1(d) is a high-resolution image recorded along the $[001]$ direction. The image shows clusters of lattice fringes that differ in contrast with the neighboring clusters of fringes. There is little thickness difference in the imaged area that could give rise to these contrast variations. The image indicates that the clusters with brighter contrast originate from those atoms that have different scattering cross section compared with the neighboring clusters of atoms. The clusters are ordered chemically distinct nano-regions. These nano-regions can cooperatively give rise to the relaxor behavior since every region would have slightly different electrical property from the neighboring region. In addition, such clusters represent mixed ordering that create the extra weak reflections shown in Figs. 1(a) and 1(b).

To interpret the image in Fig. 1(d), we carried out extensive image simulations under a variety of different parameters. Two superstructure models were employed. In model 1, the superstructure consists of eight ordered and eight disordered clusters distributed randomly across

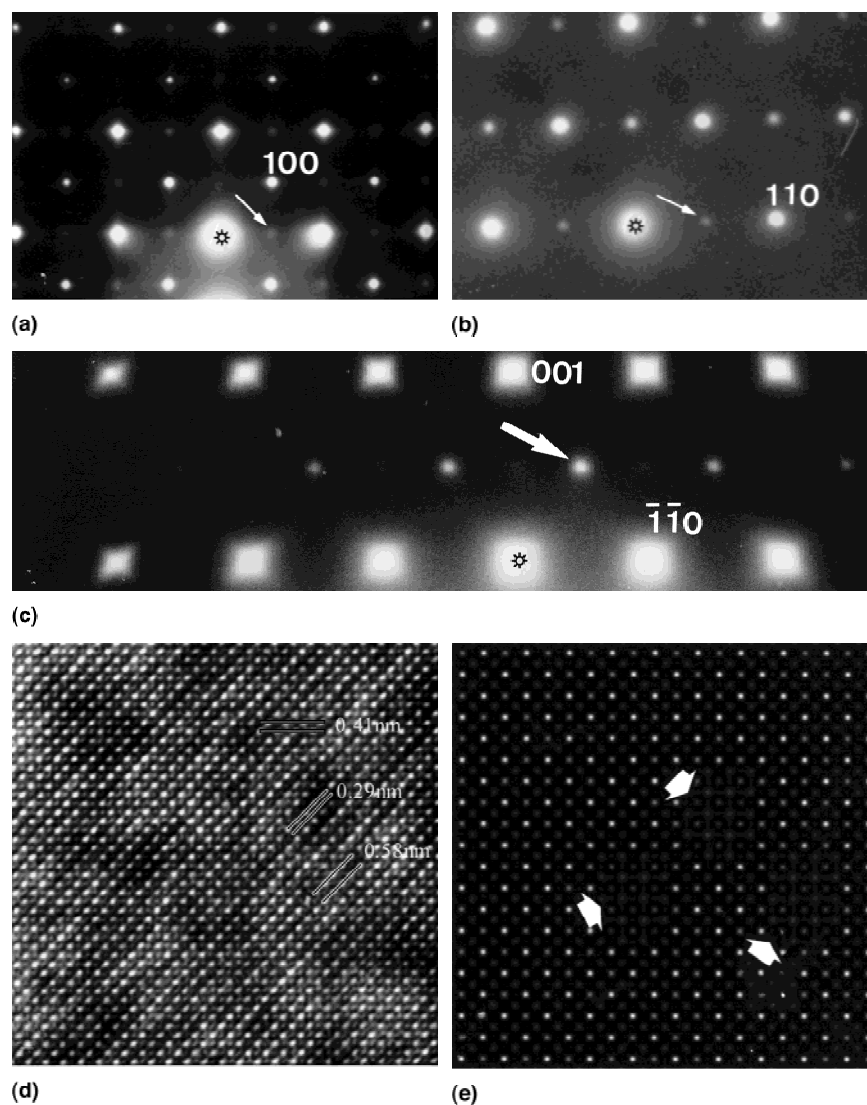


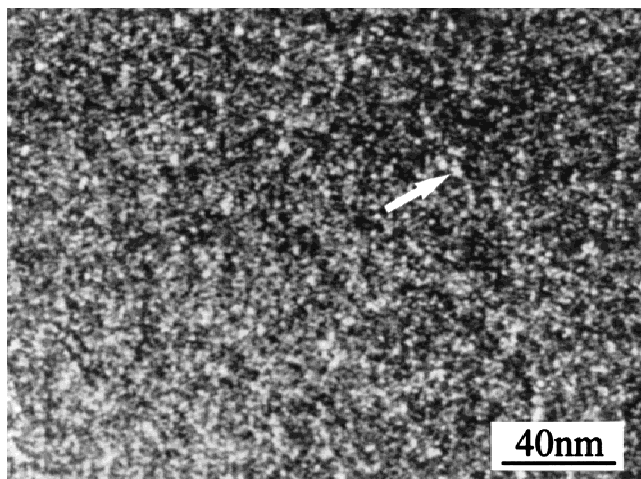
FIG. 1. (a,b) Electron diffraction patterns recorded along the $[001]$ crystal direction by TEM from grains of PST and PIM, respectively, illustrating the presence of the forbidden $1/2\ 1/2\ 0$ reflection, marked with arrows. The $1/2\ 1/2\ 0$ reflection often appears when the crystal has a high degree of structural order. Long exposure is often needed to record this reflection. (c) The diffraction pattern recorded from PIM shows the $1/2\ 1/2\ 1/2$ reflection (marked with an arrow) along the $[110]$ crystal direction, which originates from 1:1 cation ordering of the structure. (d) High-resolution TEM image showing regions of white contrast alongside those of dark contrast. The diffraction pattern in (c) originates from this region, which gives rise to the $1/2\ 1/2\ 0$ reflection. The contrast variations in the image could well arise from the presence of various cations that cluster together, creating a state of mixed order. In PIM (40/60), three different cations are capable of forming a state of mixed order. (e) Calculated image showing three regions of disordered superstructure. These are shown by arrows. The calculated image agrees well with certain regions of the HRTEM in (d), illustrating the relevance of mixed ordering along the $[001]$ direction. The distance between the bright spots is 0.58 nm.

the structure. Each cluster includes 5×5 unit cells. In model 2, the structure contains three disordered clusters, and the remaining structure is ordered. The mixed-ordered superstructure contains a total of 2200 atoms. To illustrate the relevance of mixed ordering, the simulated image in Fig. 1(e) is presented, which contains three disordered superstructures. This calculated image is in good agreement with the disordered regions of the real high-resolution electron micrograph (HREM) in Fig. 1(d). Considering the many calculations carried out, qualitatively and semi-qualitatively, the calculated

images show a realistic match between the HREM and the calculated images. The detailed results are extensive and require publication elsewhere.

Another notable aspect of the structure of PIM (40/60) is the presence of a superstructure reflection associated with structural ordering. This reflection is marked in Fig. 1(c). This reflection has been traditionally known as $1/2\ 1/2\ 1/2$ in all the Pb-based ferroelectric materials indexed with $Pm3m$. Indeed, dark-field imaging with these reflections shows structurally ordered and disordered domains that appear as dark and bright features

[Fig. 2(a)]. An interesting aspect of these domains in PIM is their unusually small size reminiscent of a partially ordered structure. However, in Pb-based ceramics, a partially ordered structure gives rise to weak superstructure reflections. In the PIM ceramics, the superstructure reflection is often very bright, as can be seen in Fig. 1(c). At this stage, it is not known what factors in PIM result in very bright superstructure reflections, which are associated with unusually small and clustered ordered domains. It should be stated that careful study of the diffraction patterns originating from the ordered regions shows streaking and diffuse scattering in the form of spirals, indicative of short-range ordering. It is considered unusual that bright superstructure reflections could originate from such disordered clusters. An example of diffuse scattering is shown in Fig. 2(b).

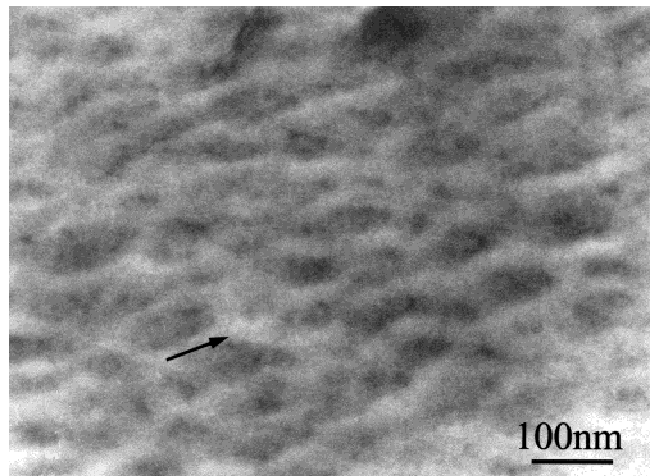


(a)

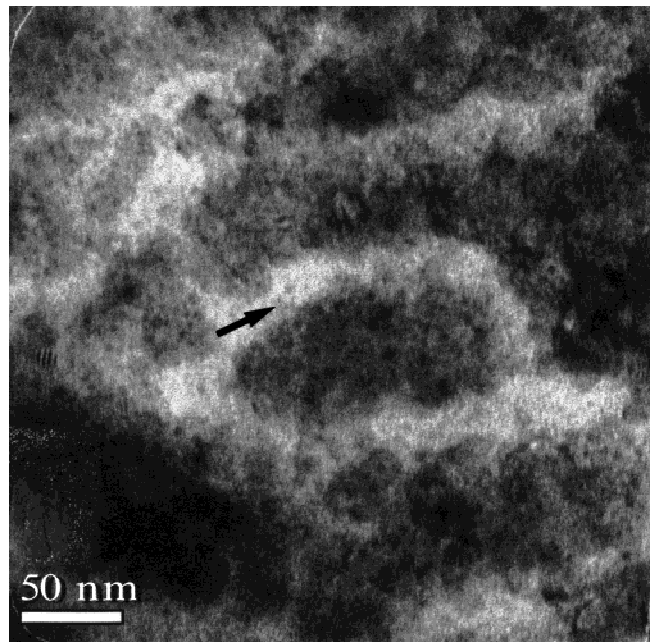


(b)

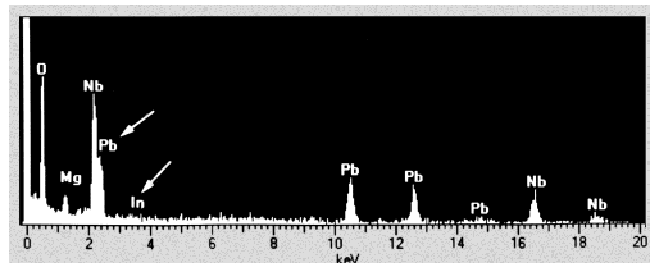
FIG. 2. (a) Dark-field image showing the configurations of the structurally ordered domains in a crystallite of PIM (40/60). The domains were imaged using $1/2\ 1/2\ 1/2$. Bright domains are ordered, whereas dark domains are disordered. The ordered domains are the small white clusters, situated within the disordered dark regions. A group of white ordered domains is illustrated with an arrow. (b) Diffraction pattern with crystal direction parallel to [110] from PIM showing the presence of diffuse scattering in the form of two spiral arms, indicating disorder and short-range order in the crystals of PIM.



(a)



(b)



(c)

FIG. 3. (a) Island features resembling domain structures in a crystal of PIM (40/60). The islands appear oriented along a certain crystal direction, but they are in fact chemically inhomogeneous regions. The white regions or boundaries are Pb deficient but can be In and Nb rich or deficient. Dark regions constitute the matrix close to the nominal but are still slightly Pb-deficient. (b) A higher magnification image illustrating the morphology of a Pb-deficient and In- and Nb-rich regions. (c) The result of x-ray microanalysis illustrating the composition of a white region which is In and Pb deficient.

Extensive studies carried out show no evidence for the presence of ferroic domain patterns in the PIM (40/60) ceramics. Domains of various features and crystallography that often occur in most ferroelectric and ferroelastic compounds were not observed in these ceramics. However, features that resemble domains were observed. An example is shown in Fig. 3(a), which shows islands separated by boundaries or walls. These boundaries appear oriented along a crystallographic direction, but subsequent studies showed that they are chemically nonstoichiometric regions with no specific crystallography. A higher-resolution image [Fig. 3(b)] obtained in TEM illustrates the irregular morphology of the boundaries. There is no specific crystallographic facet associated with this boundary. Extensive x-ray microanalysis indicated that the boundaries have significant indium and lead deficiencies, in the range 50% to 100%. They were also Nb rich on the order of 5% to 10%. X-ray microanalysis carried out indicates that the chemical compositions outside the boundaries were close to the nominal. The results of the x-ray microanalysis recorded from the white regions or boundaries are presented in

Fig. 3(c), which shows significant Pb and In deficiency. It should be stressed that 5% to 10% deficiencies in Pb were noted across all the grains, including the boundaries and their islands. The grains were therefore Pb-deficient due to the volatile nature of Pb at high temperatures. In addition to Pb-deficiency, the volatile nature of indium causes its segregation into the In-rich boundaries that exist throughout the grains. We could therefore conclude that the bright contrast of the boundaries originates from deficiencies in In, Pb, and excess Nb. X-ray diffraction indicated the presence of a peak that was indexed as pyrochlore phase. We think that the material present at the boundaries constitutes the pyrochlore phase.

Numerous inclusions of average size about 5 nm were seen dispersed across the crystallites. An example is shown in the TEM micrograph in Fig. 4(a). The image shows that these inclusions are imbedded within the grains and are crystalline. Due to their small size, it was difficult to identify their individual crystal structures, but microanalysis showed that they are mainly In- or Nb-rich inclusions. Another example, the high-resolution image in Fig. 4(b), shows the morphology, crystallinity and

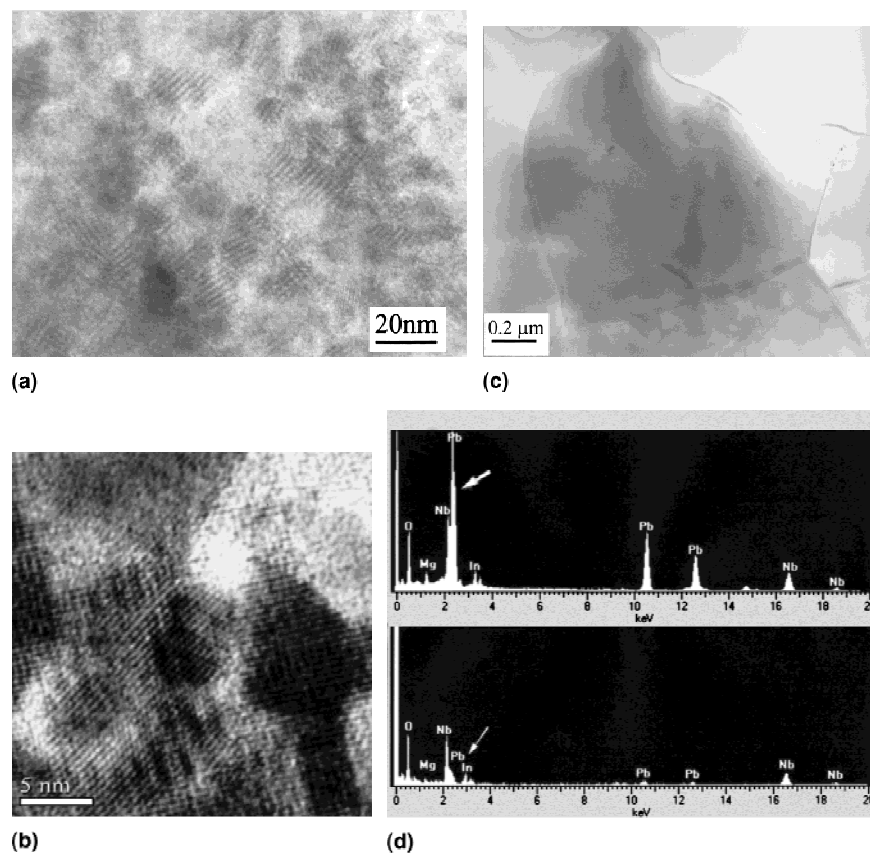


FIG. 4. (a) TEM image showing numerous nanoscale intergranular inclusions in a grain of PIM. Moiré fringes often accompany such inclusions. (b) High-resolution image showing nanoscale inclusions, their orientations and crystallinity. The white matter surrounding some inclusions is chemically inhomogeneous and nonstoichiometric material. (c) SEM micrograph showing normal crystallites in PIM. (d) X-ray microanalysis recorded in TEM illustrating. Top: composition of a normal crystallites. Bottom: the composition of an inclusion, which is highly Pb and Mg deficient.

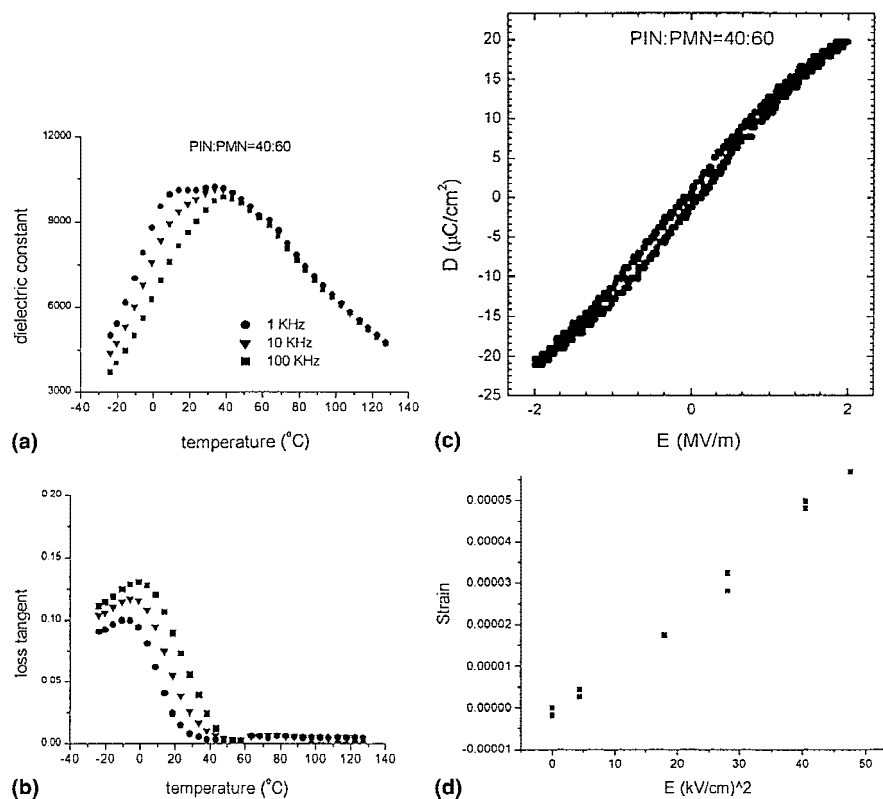


FIG. 5. The figures illustrate the electrical properties of the PIM (40/60) ceramics. (a,b) The temperature dependence of the dielectric constant and loss are illustrated. (c,d) Dielectric hysteresis loop and room temperature strain versus square of electric field, respectively. The most notable property of the ceramic, is the reduced hysteresis loop in (c).

orientations of several such inclusions. The images of the inclusions might seem similar to those of normal crystallites in a polycrystalline ceramic. The image in Fig. 4(c) is a scanning electron micrograph showing the normal crystallites in PIM. Whereas these crystallites are large, the inclusions are nanometer scale and differ in composition from the normal crystallites. The results of the x-ray microanalysis obtained in the TEM from the inclusions and the normal crystallites are presented in Fig. 4(d). It can be seen that one of the inclusions has virtually no Pb and is Mg deficient. These inclusions are intergranular and are not caused by atom milling, which can sputter tiny particulates onto the sample under certain conditions.

B. Electrical properties of PIM (40/60)

The temperature dependence of the dielectric permittivity ϵ_r and loss of (40)PIN:(60)PMN ceramics show typical relaxor behavior [Figs. 5(a) and 5(b)]. The peak in the relative permittivity shifts toward higher temperatures with increasing frequency. The transition temperature at 1 kHz is about 20 °C, at which the relative permittivity has a maximum value 10000. At 1 kHz, the loss tangent at maximum is 0.1 and increases slightly with increasing frequency. The temperature of the

loss peak shifts from -7 to 0 °C when the frequency changes from 1 to 100 kHz. Hysteresis measurements were performed at room temperature using a modified Sawyer–Tower circuit at a frequency of 50 Hz and a maximum electrical field of 2 MV/m [Fig. 5(c)]. A very slim loop and nonlinear behavior at high field were observed, revealing relaxor behavior.

The maximum polarization reached was $20 \mu\text{C}/\text{cm}^2$ while the remnant polarization was less than $2 \mu\text{C}/\text{cm}^2$. The electromechanical strain was measured using a laser interferometer, and the maximum field applied was 7 kV/cm [Fig. 5(d)]. The strain shows nonhysteresis behavior and varies with the square of the electrical field. The field-related electrostrictive coefficient M_{11} was calculated as $1.2 \times 10^{-16} \text{ m}^2/\text{V}^2$, which is of the same order of magnitude as those of the best PMN-relaxor solid solutions. The polarization related electrostrictive coefficient Q_{11} , calculated according to the relation $Q_{11} = M_{11}/\epsilon^2$, was $1.5 \times 10^{-2} \text{ m}^4/\text{C}^2$.

IV. CONCLUSIONS

Electron microscopy studies of PIM(40/60) revealed strong $1/2 \ 1/2 \ 0$ reflections that are forbidden when referred to the space group $Pm3m$. The presence of these reflections indicates substantial mixed ordering of the

B-site cations. It appears that the space group above the Curie temperature is much lower than $Pm3m$. In addition, a superstructure reflection, $1/2\ 1/2\ 1/2$, associated with the structurally ordered domains was observed. This again indicates the existence of B-site cation ordering along the $[111]$ direction when referring to cubic symmetry. The B-site ordering differs from the mixed ordering, which is related to the forbidden reflections. Diffuse scattering and irregular streaking were observed, indicating short-range order throughout the crystals.

Significant compositional anomalies were observed. These compositional variations were confined to specific clusters that were In and Pb deficient and Nb rich. It is concluded that the pyrochlore phase is associated with these clusters. In addition to the clusters of various chemical compositions, nanoscale intergranular inclusions were observed. These nanoscale inclusions originated from unreacted precursor particles, indicative of the complexity of the synthesis procedure used to fabricate the ceramics. A surprising aspect of the study was the lack of any form of domains that are often found in ferroelectric or piezoelectric relaxor compounds.

Electrical characterization of PIM (40/60) allowed a good understanding of the dielectric properties of this compound. These studies showed reduced hysteresis and aging effects in this compound when tested for electrostrictive and piezoelectric properties.

Future work will include systematic studies of the electrical properties and structural and microstructural characteristics of the entire series of $(x)\text{Pb}_2(\text{In,Nb})\text{O}_6:(1-x)\text{Pb}(\text{Mg}_{1/3}\text{Nb}_{2/3})\text{O}_3$. The compositions will vary from PIM (10/90) up to (90/10). The emphasis will be placed on improved synthesis of the morphotropic boundary phases PIM (40/60), (35:65), and (45:55) with an aim to establish the optimized compound with the most reduced hysteresis property for actuator applications.

ACKNOWLEDGMENT

This work was supported by the Centre for Smart Materials of the Hong Kong Polytechnic University.

REFERENCES

1. R. Newnham, *MRS Bull.* **XXII**, **22**, 20 (1997).
2. K. Roleder, *Key Eng. Mat.* **155–156**, 123 (1998).
3. Y. Xu, *Ferroelectric Materials and Their Applications*, (Amsterdam, North-Holland, The Netherlands, 1991).
4. T.R. Shrout, Z.P. Chang, N. Kim, and S. Markgraf, *Ferroelectric Lett.* **12**, 63 (1990).
5. Z.G. Ye and M. Dong, *J. Appl. Physics* **87**, 2312 (2000).
6. K.Z. Baba-Kishi, G.K.H. Pang, C.L. Choy, H.L.W. Chan, H. Luo, Q. Yin, and Z. Yin, *ISFE-6, The Sixth International Symposium on Ferroic Domains and Mesoscopic Structures*, edited by D. Feag and J.M. Liu (Gordon and Breach, United Kingdom, 2000), p. 611.
7. N. Setter and L.E. Cross, *J. Appl. Phys.* **51**, 4356 (1980).
8. C.G.F. Stenger and S.J. Burgraf, *Phys. Status Solidi A* **61**, 275 (1980).
9. K.Z. Baba-Kishi and D.J. Barbar, *J. Appl. Cryst.* **23**, 43 (1990).
10. K.Z. Baba-Kishi, G. Cressey, and R.J. Cernik, *J. Appl. Crystallogr.* **25**, 477 (1992).
11. P.M. Woodward and K.Z. Baba-Kishi, *ISAF XI 98 Int. Symp. on Applications of Ferroelectrics*, Montreux, Aug., edited by E. Colla, D. Damjanovic, and N. Setter (1998), p. 449.
12. K.S. Knight and K.Z. Baba-Kishi, *Ferroelectrics* **173**, 341 (1995).
13. K.Z. Baba-Kishi, in *Proc. XVII Conf. on Appl. Cryst.*, edited by H. Morawiec and Danuta Stroz (World Scientific, Singapore, 1997), p. 333.
14. S.L. Swartz and T.R. Shrout, *Mater. Res. Bull.* **17**, 1245 (1982).
15. E.F. Alberta and A.S. Bhalla, *Mater. Lett.* **40**, 114 (1999).
16. K. Nomura, H. Terauchi, N. Yasuda, and H. Ohwa, *J. Korean Phys. Soc.* **32**, S989 (1998).